Black hole formation and growth with non-Gaussian primordial density perturbations

Mélanie Habouzit, Marta Volonteri, Muhammad Latif, Takahiro Nishimichi,
Sébastien Peirani, Yohan Dubois, Gary A. Mamon, Joseph Silk, Jacopo
Chevallard

▶ **To cite this version:**

Mélanie Habouzit, Marta Volonteri, Muhammad Latif, Takahiro Nishimichi, Sébastien Peirani, et al.. Black hole formation and growth with non-Gaussian primordial density perturbations. Monthly Notices of the Royal Astronomical Society, 2016, 456 (2), pp.1901-1912. 10.1093/mnras/stv2740 . hal-01311404

HAL Id: hal-01311404

https://hal.sorbonne-universite.fr/hal-01311404v1

Submitted on 29 Aug 2022

HAL is a multi-disciplinary open access archive for the deposit and dissemination of scientific research documents, whether they are published or not. The documents may come from teaching and research institutions in France or abroad, or from public or private research centers.

L'archive ouverte pluridisciplinaire **HAL**, est destinée au dépôt et à la diffusion de documents scientifiques de niveau recherche, publiés ou non, émanant des établissements d'enseignement et de recherche français ou étrangers, des laboratoires publics ou privés.

Black hole formation and growth with non-Gaussian primordial density perturbations

Mélanie Habouzit,[1]★ Marta Volonteri,[1]★ Muhammad Latif,[1]★ Takahiro Nishimichi,[2,3]
Sébastien Peirani,[1] Yohan Dubois,[1] Gary A. Mamon,[1] Joseph Silk[1,4]
and Jacopo Chevallard[5]

[1]*Institut d'Astrophysique de Paris, Sorbonne Universités, UPMC Univ Paris 6 et CNRS, UMR 7095, 98 bis bd Arago, F-75014 Paris, France*
[2]*Kavli Institute for the Physics and Mathematics of the Universe, The University of Tokyo Institutes for Advanced Study, 5-1-5 Kashiwanoha, Kashiwa 277-8583, Japan*
[3]*CREST, JST, 4-1-8 Honcho, Kawaguchi, Saitama 332-0012, Japan*
[4]*Department of Physics and Astronomy, The Johns Hopkins University Homewood Campus, Baltimore, MD 21218, USA*
[5]*Scientific Support Office, Directorate of Science and Robotic Exploration, ESA/ESTEC, Keplerlaan 1, NL-2201 AZ Noordwijk, the Netherlands*

ABSTRACT

Quasars powered by massive black holes (BHs) with mass estimates above a billion solar masses have been identified at redshift 6 and beyond. The existence of such BHs requires almost continuous growth at the Eddington limit for their whole lifetime, of the order of one billion years. In this paper, we explore the possibility that positively skewed scale-dependent non-Gaussian primordial fluctuations may ease the assembly of massive BHs. In particular, they produce more low-mass haloes at high redshift, thus altering the production of metals and ultraviolet flux, believed to be important factors in BH formation. Additionally, a higher number of progenitors and of nearly equal-mass halo mergers would boost the mass increase provided by BH–BH mergers and merger-driven accretion. We use a set of two cosmological simulations, with either Gaussian or scale-dependent non-Gaussian primordial fluctuations to perform a proof-of-concept experiment to estimate how BH formation and growth are altered. We estimate the BH number density and the fraction of haloes where BHs form, for both simulations and for two popular scenarios of BH formation (remnants of the first generation of stars and direct collapse in the absence of metals and molecular hydrogen). We find that the fractions of haloes where BHs form are almost identical, but that non-Gaussian primordial perturbations increase the total number density of BHs for both BH formation scenarios by a factor of 2. We also evolve BHs using merger trees extracted from the simulations and find that both the mean BH mass and the number of the most massive BHs at $z = 6.5$ are up to twice the values expected for Gaussian primordial density fluctuations.

Key words: galaxies: evolution – galaxies: formation – early Universe.

1 INTRODUCTION

Primordial density perturbations evolve with time, cause the collapse of dark matter (DM) haloes and lead to the formation of large-scale structures. As the hot big bang theory has no explanation for the distribution of these density fluctuations, inflation has been considered to be a natural physical process able to produce the necessary spectrum of the density perturbations. The simplest inflationary models, a single scalar field slowly rolling down a shal-low potential, predict a very nearly Gaussian distribution of these density fluctuations (Gangui et al. 1994; Acquaviva et al. 2003; Maldacena 2003). Primordial density perturbations place the tightest constraints on inflationary models and on how physical processes at very high energies shaped the Universe at very early times.

Primordial perturbations described by a Gaussian distribution are supported, on large scales, by measurements of the temperature anisotropies of the cosmic microwave background (CMB), which are the relics of density perturbations in the cosmic fluid at the time of last scattering. Planck's results (Planck Collaboration XVI 2014a) have made incomparable progresses in the accuracy of the estimated cosmological parameters and on our knowledge of

★ E-mail: habouzit@iap.fr (MH); martav@iap.fr (MV); latif@iap.fr (ML)

the beginning of the Universe. The Planck mission has, however, focused on large structures, considering primordial density perturbations on the scale of clusters. By mapping in detail the CMB on the full sky, Planck has provided very strong constraints on the local non-Gaussianities (Gangui et al. 1994) by estimating the parameter describing the quadratic coupling of the primordial perturbations (introduced by Komatsu & Spergel 2001), $f_{NL} = 2.7 \pm 5.8$ (Planck Collaboration XXIV 2014b). However, as predicted by some inflationary models, non-Gaussianities on smaller scales, beyond the reach of Planck measurements, are still conceivable.

Recent studies have shown that scale-dependent non-Gaussianities, consistent with Planck constraints at large scale, can have an important impact on structure formation on galactic scales. Habouzit et al. (2014) used cosmological DM simulations to investigate the impact of scale-dependent non-Gaussian primordial perturbations, predicted by some inflationary models (Alishahiha, Silverstein & Tong 2004; Silverstein & Tong 2004; Chen 2005). They compared five simulations: a Gaussian simulation and four simulations based on scale-dependent non-Gaussian prescriptions for the initial conditions (all consistent with Planck's constraints). The non-Gaussian initial models developed of Habouzit et al. (2014) employed a low level of non-Gaussianities on scales of galaxy clusters and larger ($\log(f_{NL}^{local}) < 1$ for $\log(k/\mathrm{Mpc}^{-1}) < 0.75$, to be consistent with Planck's results) and a higher level on smaller scales ($\log(f_{NL}^{local}) > 1$ for $\log(k/\mathrm{Mpc}^{-1}) < -0.5$). Applying a galaxy formation model using the redshift-dependent stellar-halo mass relation of (Behroozi, Wechsler & Conroy 2013) to paint galaxies on DM haloes, Habouzit et al. (2014) find that, with non-Gaussian initial conditions, there is a significant enhancement (up to 0.3 dex at redshift ≥10) of the halo and galaxy mass function, which increases with redshift and decreases with halo/galaxy mass. The galaxy mass function is significantly altered when non-Gaussianity varies strongly with scale.

Using the same set of simulations, Chevallard et al. (2015) went further to address the implications of scale-dependent non-Gaussianities on cosmic reionization. They considered a modified semi-analytical galaxy formation model based on Mutch, Croton & Poole (2013) to compute the stellar mass assembly in each DM halo, and used the Bruzual & Charlot (2003) stellar population synthesis code to compute the far-UV luminosity function for different redshifts. Reionization is thought to be mainly driven by UV radiation emitted by massive stars born in the first galaxies because hydrogen ionizing photons can escape more easily from low-mass haloes than high-mass ones. The number of ionizing photons emitted by early galaxies depends on their number density, i.e. on their far-UV galaxy luminosity function. Chevallard et al. (2015) employed different reionization models (a fixed escape fraction $f_{esc} = 0.2$, and two different escape fractions varying with redshift) to investigate the ionization fraction of the Universe as a function of redshift, and concluded that in the most favourable case (strongest non-Gaussian model), the Universe can be reionized earlier, in better agreement with the electron Thomson scattering optical depth measured by Planck.

The population of black holes (BHs) powering quasars at $z > 6$ (Fan et al. 2006; Jiang et al. 2009; Mortlock et al. 2011) represent an issue similar to that of reionization. In the studies of reionization, for theory to match the measured electron Thomson scattering optical depth, it is necessary to assume that the escape fraction is $f_{esc} \sim 0.2$, much larger than observed for the typical galaxy. In a similar way, in the case of BHs, for theory to match their masses and number densities, it is necessary to assume that BHs grow almost continuously at the Eddington limit (or continuously at almost the Eddington rate) for a billion years: a massive BH with initial mass M_0 grows with time t as $M = M_0 \exp\{[(1 - \eta)/\epsilon](t/t_{Edd})\}$, where $t_{Edd} = \sigma_T c/(4\pi G m_p) = 0.45$ Gyr, η is the fraction of rest mass energy released by accretion, and $\epsilon \leq \eta$ the radiative efficiency. In thin accretion discs (Shakura & Sunyaev 1973), $\eta = \epsilon$, with ϵ ranging from 0.057 to 0.32 for BH spin ranging from 0 to 0.998. The BH masses of $z > 6$ quasars can reach 10^{10} M$_\odot$ (Wu et al. 2015), therefore constant Eddington-limited accretion for the whole Hubble time is implied if $M_0 < 10^2$ M$_\odot$ and $\epsilon \sim 0.1$. While this assumption is not impracticable, it stretches the typical properties of BHs and quasars. It is therefore worthwhile to assess whether scale-dependent non-Gaussianities can increase BH growth as they boost reionization powered by galaxies.

The formation and growth of BHs in a cosmology including non-Gaussian primordial density fluctuations can be altered in several ways. In the first place, a larger number of galaxies may be able to form a BH. Most theories (for a review, see Volonteri 2010, and references therein) link BH formation to the first generation of galaxies, either via the first stars (Pop III stars, stars without heavier elements than hydrogen and helium, Madau & Rees 2001; Volonteri, Madau & Haardt 2003), via gas collapse in metal-free haloes illuminated by strong photodissociating flux ('direct collapse', DC, Loeb & Rasio 1994; Bromm & Loeb 2003; Begelman, Volonteri & Rees 2006; Spaans & Silk 2006; Dijkstra et al. 2008; Latif et al. 2013), or via mergers of stars or stellar-mass BHs in dense stellar clusters (Devecchi & Volonteri 2009; Davies, Miller & Bellovary 2011). The formation of BHs in the cosmology we propose could be impacted in two ways; the enhancement at the low-mass end of the galaxy mass function at high redshift could increase the number of haloes producing stars, thus boosting the formation of BHs as Pop III remnants. Regarding the DC scenario, the number of haloes illuminated by dissociating radiation could also be enhanced because of the higher star formation. On the other hand, the enhanced stellar production would also lead to increased metal pollution, suppressing the 'eligibility' of a fraction of haloes. Therefore, some BH formation mechanisms would be boosted, and other may be suppressed in a way non-trivial to predict.

The growth of BHs is also impacted. There are two channels for BHs to grow in mass: the first one is by BH–BH mergers, the second one by accretion of gas, which can be strongly increased during galaxies merger episodes. Both channels are facilitated in the presence of non-Gaussianities, because of the increased number of low-mass galaxies, which increases the number of galaxy mergers, and of BH mergers as well.[1]

In this paper, we compare the formation and growth of BHs in a Gaussian simulation and the most non-Gaussian simulation of Habouzit et al. (2014), G and NG4 thereafter. In Section 2, we recall the main features of the two simulations using initial conditions with either Gaussian or non-Gaussian primordial perturbations. In Sections 3 and 4, we investigate the formation of BHs through two formation scenarios: DC (Section 3) and the remnants of the first generation of stars (Section 4). We build a model to compute the Lyman–Werner (LW) radiation that may impinge on each halo in the two simulations. Looking at all haloes evolving under a radiation higher than $J_{21,crit}$, we are able to estimate where DC BHs can form for the two simulations. Similarly, Section 4 is devoted to the

---

[1] A small fraction of merging BHs may however be ejected from the host haloes because of the gravitational wave induced recoil, (e.g. Redmount & Rees 1989; Schnittman 2007) thus lowering the 'positive' contribution of BH–BH mergers.

study of the number density of BHs formed via the remnants of the first generation of stars. In Section 5, we follow the most massive haloes in both simulations with the aid of merger trees to perform an analysis addressing the growth of BHs over cosmic time.

2 SIMULATION PARAMETERS

2.1 Initial conditions: prescription for scale-dependent non-Gaussianities

We employ a simple model to have a significant amount of non-Gaussianity on small scales, relevant for early structure formation, while keeping them small on large scales to meet the strong constraints obtained by the Planck CMB mission (Planck Collaboration XXIV 2014b). Namely, we investigate here the *generalized local ansatz* proposed by Becker, Huterer & Kadota (2011):

$$\phi(\boldsymbol{x}) = \phi_{\rm G}(\boldsymbol{x}) + \left[f_{\rm NL} * (\phi_{\rm G}^2 - \langle \phi_{\rm G}^2 \rangle) \right] (\boldsymbol{x}), \tag{1}$$

where $\phi(\boldsymbol{x})$ is the curvature perturbation, $\phi_{\rm G}$ a Gaussian random field and where the operation $(f_{\rm NL} * A)$ is a convolution of a random variable A and a k-dependent kernel defined in Fourier space:

$$f_{\rm NL}(k) = f_{\rm NL,0} \left(\frac{k}{k_0} \right)^{\alpha}. \tag{2}$$

We explore four different models by varying the normalization $f_{\rm NL,0}$ and the slope α of $f_{\rm NL}(k)$, in such a way that the non-Gaussianity is significant on galactic scales, yet small enough to meet the current constraints from the Planck mission (Planck Collaboration XXIV 2014b). We restrict ourselves to positively skewed primordial density fluctuations, i.e. $f_{\rm NL} > 0$, hence $f_{\rm NL,0} > 0$.

We modify the initial condition generator originally developed by Nishimichi et al. (2009), based on second-order Lagrangian perturbation theory (e.g. Scoccimarro 1998; Crocce, Pueblas & Scoccimarro 2006), parallelized by Valageas & Nishimichi (2011) and with local-type non-Gaussianities implemented by Nishimichi (2012). We follow Becker et al. (2011) and realize the generalized local ansatz of equation (1) by taking a convolution of the curvature squared and the k-dependent $f_{\rm NL}$ kernel in Fourier space. We use the public Boltzmann code, CAMB (Lewis, Challinor & Lasenby 2000) to compute the transfer function and multiply it to the curvature perturbations to have the linear density fluctuations.

2.2 *N*-body simulations, halo catalogue, and merger trees

We have performed five cosmological simulations with GADGET-2 (Springel 2005) for a Λ cold dark matter universe using Planck parameters (Planck Collaboration XVI 2014a), namely $\Omega_{\rm m} = 0.307$, $\Omega_{\Lambda} = 0.693$, $h = 0.678$, $\sigma_8 = 0.829$, and $n_{\rm s} = 0.9611$. Each simulation was performed in a periodic box of side $50\,h^{-1}$ Mpc with 1024^3 DM particles (e.g. with mass resolution of $\sim 9.9 \times 10^6\,h^{-1}\,{\rm M}_\odot$). One simulation uses Gaussian initial conditions (hereafter, 'G'), while the others consider non-Gaussian initial conditions (in this work, only the most powerful non-Gaussian simulation, 'NG4' is used, equations 1 and 2). For simulation G, we use $f_{\rm NL,0} = 0$, while simulation NG4 is described by $f_{\rm NL,0} = 10^4$ and $\alpha = 4/3$ (see equation 2), both simulations with the same initial phases. The simulations started at $z = 200$ and ended at $z = 6.5$. In each case, the Plummer-equivalent force softening adopted is 5 per cent of the mean interparticle distance ($2.44\,h^{-1}$ kpc), kept constant in comoving units.

For each snapshot (taken every ~ 40 Myr), catalogues of haloes are prepared using ADAPTAHOP (Aubert, Pichon & Colombi 2004)
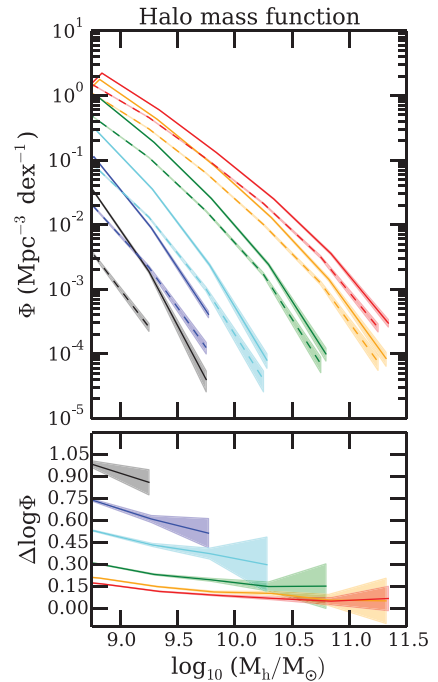
Figure 1. Halo mass functions (top panel) for the Gaussian G (dashed lines) and non-Gaussian NG4 (lines) simulations. Residual of the log mass function between Gaussian and non-Gaussian simulations is shown on the bottom panel. The different curves indicate different redshifts: $z = 17$ (black), $z = 15$ (blue), $z = 13$ (cyan), $z = 10$ (green), $z = 8$ (orange), $z = 7$ (red).

which uses an SPH-like kernel to compute densities at the location of each particle and partitions the ensemble of particles into subhaloes based on saddle points in the density field. The use of this code is then attractive, since subhaloes are separated from their parent haloes. Note that, in our study, only haloes or subhaloes containing at least 20 particles (i.e. $2.9 \times 10^8\,{\rm M}_\odot$) were retained in the different catalogues. We then study the individual evolution of (sub)haloes, by building halo merger trees using TREEMAKER (Tweed et al. 2009). This latter allows us to obtain the evolution of physical properties of each (sub)halo, such as the mass and the list of all of its progenitors. Thus, one can derive accurately the evolution of the mass of each DM (sub)halo.

Fig. 1 shows the halo mass function for the Gaussian (G, dashed lines) and the non-Gaussian (NG4, solid lines) simulations as a function of the virial halo mass, for different redshifts from $z = 17$ to $z = 7$ (see also Habouzit et al. 2014). The main conclusion is that primordial non-Gaussianities introduce an enhancement in the halo mass function, which increases with redshift and decreased with halo mass. At $z = 10$ (green curves, bottom plot), this enhancement is up to 0.3 dex. The consequences of positively skewed non-Gaussian initial conditions with a blue tilt (i.e. $\alpha > 1$) are that the formation of less massive haloes are amplified more significantly. This is simply because the formation of these haloes originate from initial fluctuations on small scales (i.e. large k) where we put more non-Gaussianity. Then, the mode transfer from large to small scales through the non-linear nature of structure formation driven by gravitational instability gradually surpasses the initial signal on small scales, resulting in the suppression of the halo mass function ratio with time (see bottom panel of Fig. 1). At redshift $z = 7$, the ratio is 0.15 dex or smaller. A similar halo abundance at the final time but with initially very different halo mass function naturally indicates that the merger history is different in the two

simulations. It is thus well motivated to go beyond the simple halo abundance comparison and consider the evolution of BH mass in detail by following the merger history of each halo. Since such investigation is difficult with analytical calculation, we here resort to numerical simulations and build a simple model for the formation and the evolution of BHs.

3 MODELLING THE LW RADIATION TO ESTIMATE THE DISTRIBUTION OF POTENTIAL DC BHS

In this section, we study whether the probability of forming BHs in the DC scenario (Loeb & Rasio 1994; Bromm & Loeb 2003; Koushiappas, Bullock & Dekel 2004; Begelman et al. 2006; Lodato & Natarajan 2006; Dijkstra et al. 2008; Latif et al. 2013) is higher or lower when scale-dependent non-Gaussianities produce more low-mass haloes. The DC scenario is very appealing as it may lead to the formation of large 10^4–10^6 $M_\odot$ seeds, that ease the growth constraints for the sample of $z > 6$ quasars.

Metal-free haloes at high redshift ($z = 20$ and later) may host the formation of DC BHs under specific conditions. If the inflow rate of gas at the centre of the halo is higher than $0.1\,M_\odot\,yr^{-1}$, a supermassive star-like object (Begelman et al. 2006; Spaans & Silk 2006; Begelman, Rossi & Armitage 2008; Begelman 2010; Ball et al. 2011) forms in the nucleus, and this star collapses and forms a BH with mass up to 90 per cent of the stellar mass. Metals, able to efficiently cool the gas to low temperatures, down to CMB temperature, would strongly decrease the Jeans mass, thus fostering fragmentation and star formation, decreasing the inflow rate needed to form only one massive object in the centre of the gas cloud. The presence of molecular hydrogen could also cool the gas; a strong photodissociating radiation (LW, photons $11.2\,eV < E_{LW\,photons} < 13.6\,eV$) is then needed to destroy molecular hydrogen and prevent its formation. The conditions advocated for DC models are therefore: metal-free conditions and presence of a sufficiently strong dissociating LW flux.

The level of 'critical' LW radiation is a major factor in the DC BH scenario. Several aspects have been addressed in the last years. Despite the fact that the mean LW radiation background is orders of magnitude lower than the radiation intensity required to keep the fraction of molecular hydrogen close to zero ($<10^{-4}$), spatial variations in the LW intensity appear to be a key element in the DC mechanism (Dijkstra et al. 2008). Using simulations and an analytic framework, Shang, Bryan & Haiman (2010), Ahn et al. (2008), Agarwal et al. (2012), and Agarwal et al. (2014) find that spatial variations in the LW radiation exist and are due to clustering of the LW photon sources and the matter density fluctuations (large-scale structures): the proximity with star-forming regions is essential for the DC scenario. These studies suggest that a halo can be exposed to a high enough LW radiation intensity if it lives in a clustered environment, close to star-forming galaxies. Dijkstra et al. (2008) compute the probability distribution function of the LW radiation that irradiates haloes at redshift $z = 10$ and show that a small fraction of haloes (10^{-8}–10^{-6}) can be exposed to a radiation higher $J_{21,LW,crit} \sim 10^3$ (in units of $10^{-21}\,erg\,s^{-1}\,cm^{-2}\,Hz^{-1}\,sr^{-1}$), a value shown by Bromm & Loeb (2003) to lead to a sufficiently low molecular hydrogen fraction. Dijkstra, Ferrara & Mesinger (2014, D14 hereafter) suggest that the number density of DC BHs is sufficient to explain that of $z > 6$ quasars if $J_{21,LW,crit} \sim 10^2$.

In the meanwhile, Latif & Volonteri (2015) use zoomed cosmological simulations of single haloes to find that complete molecular hydrogen dissociation may not be necessary, while Latif et al.

(2015) and Inayoshi & Tanaka (2015) include the impact of X-rays on molecular hydrogen dissociation and show that X-rays make DC BHs rarer than previously expected, less than the number density of $\sim 1\,Gpc^{-3}$ necessary to explain the population of $z > 6$ quasars. However, non-Gaussianities provide an enhancement in the low-mass end of the halo/galaxy mass function, therefore they can increase the probability of having halo/galaxy clustered regions, hence boosting the number density of eligible DC regions in the early Universe.

3.1 The model

Our model is a modification of D14, where we adopt DM simulations to obtain the clustering of haloes and their redshift evolution, rather than analytical prescriptions (see Inayoshi & Tanaka 2015, for a discussion of the uncertainties in clustering assumptions). To identify haloes which can potentially form a DC BH we use the LW radiation model of D14, described in the following.

The stellar mass of a DM halo M_h is assigned as

$$M_\star = f_\star M_{h,gas} = f_\star \frac{\Omega_b}{\Omega_m} M_h, \tag{3}$$

where $f_\star = 0.05$ is the fraction of gas which turns into stars, $M_{h,gas}$ the gas mass of the halo, M_h the total mass of the halo, Ω_b the baryon density, and Ω_m the total matter density. The mean production rate of LW photons per solar mass of star formation is time-dependent, where time is counted from the time t_{Myr} when a burst of star formation occurs, and expressed as

$$\langle Q_{LW}(t) \rangle = Q_0 \left(1 + \frac{t_{Myr}}{4} \right)^{-3/2} \exp\left(-\frac{t_{Myr}}{300} \right) \quad s^{-1}\,M_\odot^{-1}. \tag{4}$$

with $Q_0 = 10^{47}\,M_\odot\,s^{-1}$.

The mean production rate is computed one free-fall time after the star formation burst. Assuming that $t_{ff} = \sqrt{3\pi/(32\,G\,\rho)} = \sqrt{3\pi/(32\,G\,200\,\rho_c)} = \sqrt{3\pi/(32\,G\,200\,(1+z)^3\,\rho_{c,0})}$, the free-fall time can be expressed as

$$t_{Myr,ff} \sim 83 \left(\frac{1+z}{11} \right)^{-3/2}. \tag{5}$$

D14 motivate this choice by the requirement that the molecular hydrogen is suppressed throughout the collapse. The expression of Q_{LW} is a fit from STARBURST99 (which used a Salpeter initial mass function in the range $m_{low}, m_{up} = 1100\,M_\odot$, an absolute metallicity of $Z = 10^{-3}$ (0.05 $Z_\odot$), and a stellar mass of $10^5\,M_\odot$). The mean LW luminosity density $\langle L_{LW}(M, t) \rangle$ is a function of the mean number of LW photons (given by the mean production rate of LW photons per solar masses times the stellar mass of the halo), their energy and the escape fraction of these photons (we assume $f_{esc} = 1$ in this study to be able to compare with the fiducial model of D14):

$$\langle L_{LW}(M, t) \rangle = \frac{h \langle \nu \rangle}{\Delta \nu} \langle Q_{LW}(t) \rangle f_{esc,LW} \left(\frac{M_\star}{M_\odot} \right). \tag{6}$$

The flux at a distance r then becomes:

$$\langle J_{LW}(r, M, t_{ff}) \rangle = \frac{1}{4\pi} \frac{\langle L_{LW}(M, t) \rangle}{4\pi r^2} f_{mod}(r), \tag{7}$$

where the first factor $1/4\pi$ is required to express $\langle J_{LW}(r, M, t_{ff}) \rangle$ in J_{21} units (erg s^{-1} cm^{-2} Hz^{-1} sr^{-1}). $f_{mod}(r)$ is used to correct the radiation intensity for the extra dimming introduced by the LW

horizon (Ahn et al. 2008):

$$f_{\mathrm{mod}}(r) = 1.7 \exp\left(-\left(\frac{r_{\mathrm{cMpc}}}{116.29\alpha}\right)^{0.68}\right)$$
$$-0.7 \quad \text{if } r_{\mathrm{cMpc}}/\alpha \leq 97.39 \tag{8}$$

$$= 0 \quad \text{otherwise.} \tag{9}$$

Where the size is expressed in comoving Mpc (cMpc). We assume in our study that each halo has a 10 per cent probability of being star forming for all redshifts, $P_{\mathrm{SF}} = 0.1$, in agreement with Dijkstra et al. (2008). Therefore, only 10 per cent of the haloes in the box are considered to compute the radiation intensity, and only 10 per cent of nearby haloes contribute to this radiation intensity. Haloes are chosen randomly. The experiment is repeated 40 times to take into account the random choice of haloes which are flagged as star forming.

Two main opposite factors influence the number of potential eligible DC regions: the LW radiation intensity coming from nearby star-forming regions illuminating haloes and the metal pollution they can be exposed to. Haloes irradiated by the LW flux coming from a nearby star forming halo can also be polluted by metals released at the end of the lives of the same stars which produce the radiation. Haloes that are metal-enriched would be able to cool too efficiently to be potential DC regions anymore. The metal pollution of a halo can come from three different contributions: (i) the contamination by the halo itself if it is star forming, (ii) the contamination from the past history of the halo, and (iii) the potential contamination by close star-forming regions because of supernova (SN)-driven galactic winds which spread metals in their surroundings.

To account for the first source of pollution (i), we eliminate from the list of potential DC candidates the haloes which are star forming at the current time, with the probability of being star-forming $P_{\mathrm{SF}} = 0.1$ as described above. To account for the second contamination (ii), we estimate the probability that a halo had a progenitor which was star forming in the past. In a hierarchical theory of structure formation, haloes are formed through the continuous merging of smaller structures, which may have already encountered SN-driven metal-enrichment episodes, making the present halo metal polluted. Therefore, the probability for a halo to be metal polluted increases with the number of their progenitors. For a halo of a given mass and at a given redshift, the number of progenitors is on average larger for NG4 (dashed curves), than for G. For instance, at $z = 15$ haloes with mass $10^{10} - 3.16 \times 10^{10}\,\mathrm{M_\odot}$ have a 50 per cent probability of having less than five progenitors in G, and a 50 per cent probability of having less than 10 progenitors in NG4. In order to account for this effect we compute the mean number of progenitors per halo, for different halo mass bins, and redshifts, shown in Fig. 2. The mean number of progenitors is derived from the merger trees described in Section 2.2.

The probability for a halo to be metal polluted by heritage, i.e. to have metal-polluted progenitors $P_{\mathrm{SF\,progenitor}}|_{M_{\mathrm{h}},z}$ is described by

$$P_{\mathrm{SF\,progenitor}}|_{M_{\mathrm{h}},z} = P_{\mathrm{SF}} \times \langle\text{number of progenitors}\rangle\,|_{M_{\mathrm{h}},z}. \tag{10}$$

We keep as potential DC candidates only those haloes which, after Monte Carlo sampling this probability, result metal free.

Regarding the last source of metal pollution (iii), D14 conclude that metal pollution from nearby galaxies, through galactic winds, could be an important aspect of the halo candidates contamination. Including the redshift dependence of density and free-fall time in the expression provided by D14 for the bubble radius, in proper kpc
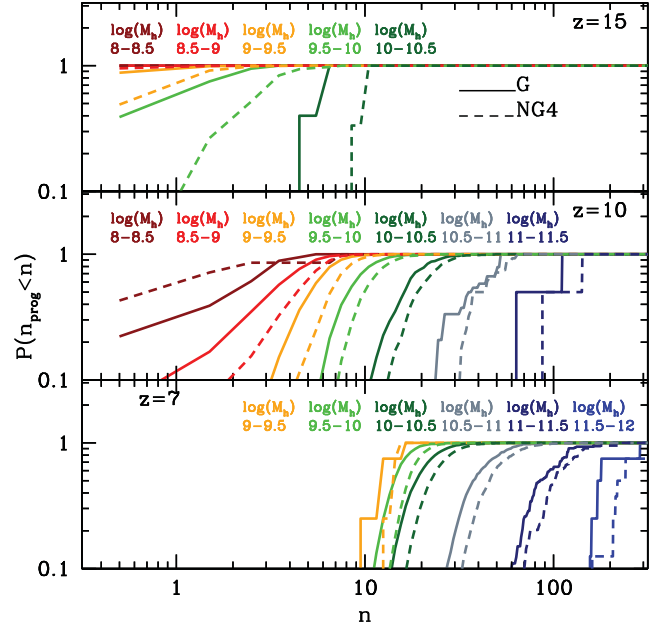
Figure 2. Probability of having given number of progenitors for haloes in a given mass range and at a given redshift ($z = 15$, $z = 10$, $z = 7$ from the top to the bottom panel). The Gaussian simulation is represented with lines, whereas dashed lines are for the non-Gaussian simulation NG4. The typical number of progenitors is larger for NG4 at almost all masses and redshifts.

(pkpc), of a metal-polluted bubble one free-fall time after the SF burst:

$$r_{\mathrm{bubble}} = 22\,\mathrm{pkpc}\left(\frac{M_{\mathrm{h}}}{10^{11}\,\mathrm{M_\odot}}\right)^{1/5}\left(\frac{1+z}{11}\right)^{-6/5}, \tag{11}$$

while the radius r_{rad} of the sphere where $J_{21,\mathrm{LW}} = 100$ one free-fall time after the star formation burst scales as

$$r_{\mathrm{rad}} = 126\,\mathrm{pkpc} \times \left(\left(1 + \frac{83}{4}\left(\frac{1+z}{11}\right)^{-3/2}\right)^{-3/2}\right.$$
$$\times \exp\left(-\frac{83}{300}\left(\frac{1+z}{11}\right)^{-3/2}\right)\Bigg)^{1/2}$$
$$\left. \times \left(\frac{M_{\mathrm{h}}}{10^{11}\,\mathrm{M_\odot}}\right)^{1/2}\left(\frac{J_{21,\mathrm{LW}}}{100}\right)^{-1/2}\left(\frac{f_{\mathrm{mod}}}{1}\right)^{1/2}. \right. \tag{12}$$

Fig. 3 compares the radius of the metal-polluted sphere (r_{bubble}) to the sphere (r_{rad}) where $J_{21,\mathrm{LW}} = 100$ or $J_{21,\mathrm{LW}} = 300$.

A correction that accounts for galactic winds coming from nearby star-forming galaxies is then added: if the distance between the halo we are considering as a DC candidate and a SF halo is less than r_{bubble}, then the candidate halo would be metal polluted, hence not an eligible DC region anymore. Fig. 3, however, shows that only haloes with mass $\sim 10^{11}\,\mathrm{M_\odot}$ at $z > 13$ can act as catalysts of a DC process in a nearby halo if $J_{21,\mathrm{LW,crit}} \leq 100$. At lower masses and redshift the metal-polluted bubble is always larger than the bubble irradiated by sufficiently high UV flux. In our simulations, we do not have any haloes with mass $> 10^{11}\,\mathrm{M_\odot}$ at $z \geq 11$ or $> 10^{10}\,\mathrm{M_\odot}$ at $z > 16$, and for lower mass haloes at lower redshift, as shown in Fig. 3, the bubble size is larger than the sphere irradiated by $J_{21,\mathrm{LW}} = 100$ or $J_{21,\mathrm{LW}} = 300$. Adding this correction, therefore, would leave no DC candidate in the simulation box.
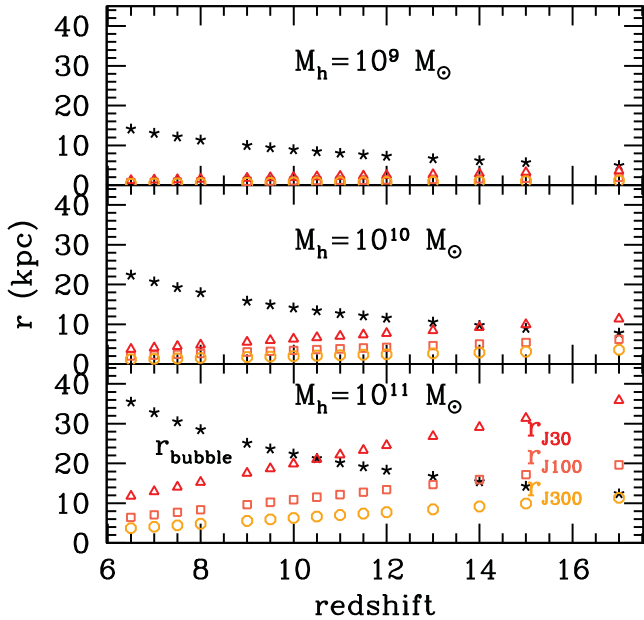
Figure 3. Metal-polluted bubble radius (black stars), and radius of the regions where $J_{21,LW} = 30$ (red triangle), $J_{21,LW} = 100$ (orange squares) or $J_{21,LW} = 300$ (yellow circles) versus redshift for different halo masses (10^9, 10^{10}, 10^{11} M$_\odot$). All quantities are computed one free-fall time after the star formation burst. Only regions which are at a distance above the distance given by r_{bubble}, and below the r_{rad} are illuminated by the given radiation intensity and are not polluted by galactic winds. For instance, haloes with mass 10^{11} M$_\odot$ at $z = 15$ can irradiate a nearby halo at a distance of ~17 kpc with an intensity $J_{21,LW} = 100$ without polluting it (the metal bubble has reached only a distance of ~14 kpc).

3.2 Results

3.2.1 Number density of potential DC regions

The number density of DC regions obtained in this study is shown in Fig. 4, for both G and NG4. Blue star symbols represent the number density of DC regions in G and green star symbols in NG4, using a model where we consider $J_{21,LW,crit} = 300$.

In Fig. 4, we also reproduce the results of the three main models used in D14: triangles correspond to their fiducial model where $J_{21,LW,crit} = 300$ and galactic wind pollution is included, circles to a model with $J_{21,LW,crit} = 100$ and galactic wind pollution, and stars to a model with $J_{21,LW,crit} = 300$ without considering galactic wind pollution. Star symbols in our study and in D14 can be directly compared as they use the same modelling for the radiation intensity. The two differences between the two studies are that we use a DM simulation to obtain the spatial distribution of haloes, rather than an analytical prescription, and that we have derived the probability for a halo to be metal free from the mean number of progenitors (from the merger tree history) in halo mass and redshift bins, whereas D14 use an analytical prescription. Despite these differences, our study is in good agreement with D14.

It is worth noting that our model does not include a treatment for galactic wind pollution (at the current time or in the past). If we included these effects, as discussed in Section 3.1, we would not identify any DC regions in our simulation boxes, in either G or NG4. Indeed, if we estimate the number of DC candidates N_{DCBH} in our simulation box from the model by D14, which includes galactic wind pollution, we find that N_{DCBH} is less than one ($N_{DCBH} = n_{DCBH} \times V_{box} \approx 10^{-7} \times V_{box} = 0.04$ with V_{box} the simulation box volume).
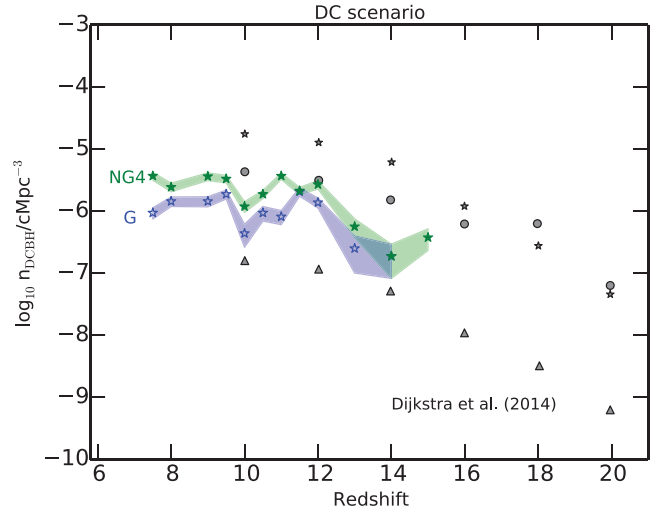

Figure 4. Number density of DC regions identified at a given redshift in the Gaussian (blue star symbols) and non-Gaussian (green star symbols) simulations. Blue and green stars are derived from a model which does not account for direct pollution by galactic outflows, and where we use the radiation intensity threshold $J_{21,LW, crit} = 300$. Shaded areas represent the Poissonian error bars derived from 40 realizations of the process. The D14 results are shown in grey symbols: triangles correspond to their fiducial model where $J_{21,LW,crit} = 300$ and account for galactic winds pollution, circles to $J_{21,LW,crit} = 100$, and stars to $J_{21,LW,crit} = 300$ without considering galactic winds pollution. Blue and green star symbols in our study can be compared with star symbols in D14 as they use the same modelling for the radiation intensity (the only differences being the probability of genetic pollution, and the use of an analytical model versus a cosmological simulation). Error bars represent the uncertainty of the mean value of the number density of BHs.

With our model, we find that NG4 (green star symbols on Fig. 4) host a number density of DC regions slightly larger than the Gaussian simulation (blue star symbols) for the whole range of redshifts, although the differences at the largest redshifts are within the $1 - \sigma$ uncertainty. The cumulative number density of BHs at redshift z=7.5 is 1.1×10^{-5} cMpc^{-3} for G, while in NG4 the cumulative number density is almost twice, with 2.3×10^{-5} cMpc^{-3}. The cumulative number densities of the two simulations differ by more than $1 - \sigma$.

While the number density of BHs in NG4 is larger, so is the number of haloes. In fact, when we estimate the occupation fraction of newly formed BHs, i.e. the fraction of haloes as a function of redshift where a BH is potentially formed (Fig. 5, this occupation fraction is not cumulative, i.e. we calculate it for newly formed BHs only) we find that the probability of a halo being seeded with a BH is almost identical in the two simulations, although at the highest redshifts the occupation fraction in the Gaussian case is slightly above the non-Gaussian one. This can be explained as follows: since the number of progenitors is larger in the non-Gaussian simulation (see Fig. 2), haloes in the non-Gaussian simulation have a higher probability of being metal polluted because of heritage pollution. In summary, scale-dependent non-Gaussianities boost the overall number of potential DC BHs in the Universe, but not the probability that a halo hosts or not a BH.

3.2.2 In the vicinity of the two most massive haloes

The analysis presented in the previous section highlights the difficulty of finding a significant number of DC regions. In order to
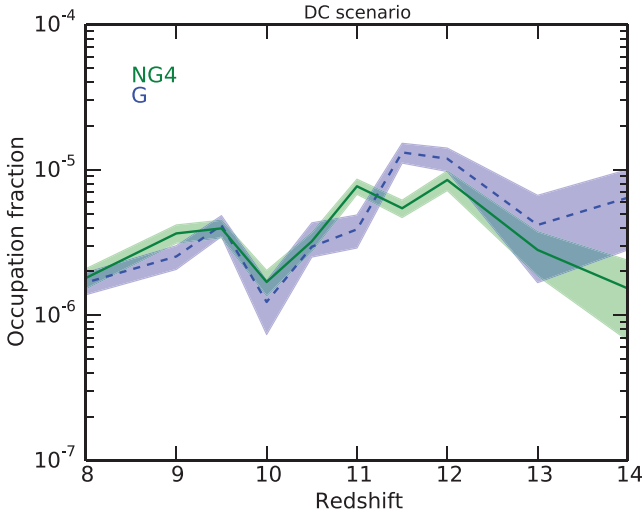
Figure 5. Halo occupation fraction of newly formed BHs for the Gaussian (dashed blue line) and non-Gaussian (solid green line) simulations, as a function of redshift, for the DC scenario (without taking into account the metal pollution from galactic winds). This is not a cumulative probability, but the probability that a BH forms in a halo at a given redshift. Error bars represent the uncertainty of the mean value of the occupation fraction.

have a clearer picture of the interplay between irradiation and metal pollution in the model by D14, we focus here on the haloes neighbouring the two most massive haloes in our simulation volume. The reason for this choice is that according to the model described in Section 3.1, only haloes more massive than 10^{11} M$_\odot$ can provide an intensity higher than $J_{21,LW} = 300$ at a distance of 10 pkpc one free-fall time after the star formation burst. Critically, a common critical intensity value suggested by simulations (Bromm & Loeb 2003; Sugimura, Omukai & Inoue 2014; Regan, Johansson & Wise 2014; Latif & Volonteri 2015) is $J_{21,LW,crit} \sim 10^3$.

We therefore select the two haloes more massive than 10^{11} M$_\odot$ at redshift $z = 10$ in the G and NG4 simulations. These two haloes match one another in the two simulations. Only these two haloes are able to produce sufficient radiation to efficiently dissociate molecular hydrogen on $\sim$20 pkpc distances. We consider all the haloes inside a 20 pkpc radius centred on each of the most massive haloes and compute the radiation intensity illuminating them.

In Fig. 6, haloes shown in red are illuminated by a radiation intensity higher than $J_{21,LW} = 500$. The number of haloes is higher for the non-Gaussian simulation, as well as the number of haloes exposed to a high radiation intensity. In NG4, which forms more low-mass haloes, the potential number of DC regions is increased. However, if we account for SN-driven metal pollution using equation (11), 1 Myr after the SN explosion, the metals in the massive halo are already spread over 4 pkpc. After 2 Myr, the metal-polluted sphere reaches 5–6 pkpc. At this time all haloes illuminated by a LW intensity $J_{21,LW} > 300$ are inside this sphere and therefore polluted by metals, making the DC process unfeasible.

Within the formalism we have adopted here, we cannot identify a difference between G and NG4. However, this model includes several simplifications, for instance the expansion of the metal bubble in a real Universe may not be spherical, and P_{SF} may well be a function of redshift and halo mass. We argue that the non-Gaussian simulation, having more low-mass haloes irradiated by a strong UV flux, could represent a more favourable environment for this scenario.
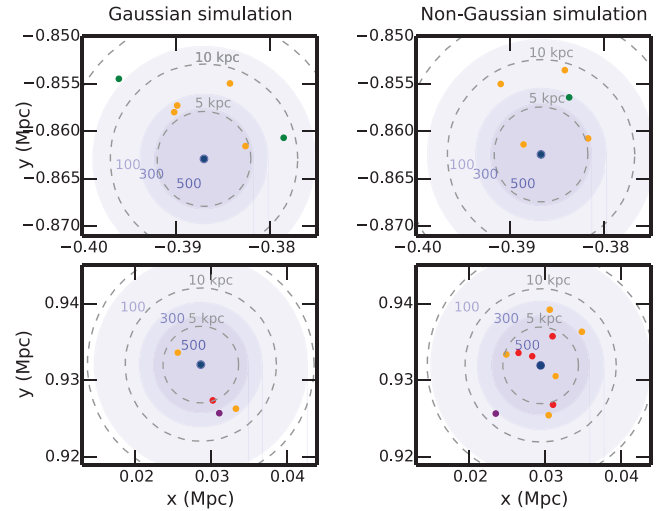
Figure 6. The two most massive haloes of the Gaussian and non-Gaussian simulations at redshift $z = 10$ are presented in blue dots. On the top-left panel, we show a halo with a mass of 1.17×10^{11} (ID 54335), on the top right 1.65×10^{11} (ID 61371), on the bottom left 1.22×10^{11} (ID 104966) and on the bottom right 1.75×10^{11} M$_\odot$ (ID 118759). Indicative radii of 5, 10, and 15 kpc are shown with grey dashed lines in the (x, y) plane. The radiation intensity from these massive haloes is shown in blue contours, the innermost area has intensity higher than $J_{21,LW} = 500$, the second by $J_{21,LW} = 300$ and outermost $J_{21,LW} = 100$. Finally, the projection of haloes in the plane (x, y) is shown in colours indicating the radiation intensity they experience (in 3D): in green $J_{21,LW} < 100$, in orange $J_{21,LW} \geq 100$, in purple $J_{21,LW} \geq 300$, in red $J_{21,LW} \geq 500$.

4 BHS FORMED FROM THE REMNANTS OF THE FIRST GENERATION OF STARS.

Pop III star remnants is another popular scenario to explain the formation of BH seeds in the early Universe (Madau & Rees 2001; Volonteri et al. 2003). BHs are predicted to form in metal-free mini-haloes ($M_h \sim 10^5$ M$_\odot$) at redshift $z = 20$–30 from the remnants of the first generation of stars (the so-called Pop III stars, which are stars without elements heavier than hydrogen and helium). These stars have never been observed so far, nevertheless they are thought to have masses ranging from 10 to 1000 M$_\odot$ (Bromm & Yoshida 2011; Hirano et al. 2015b, and references therein). If some of these stars are sufficiently massive(>260 M$_\odot$), BHs retaining up to half the stellar mass are formed, leading to the formation of a BH seed of $\sim$100 M$_\odot$ (Fryer, Woosley & Heger 2001).

In this section, we want to estimate the number density of BHs and the fraction of haloes where a BH can form via the Pop III stars scenario for G and NG4. We stress that our simulations do not have the resolution needed to resolve mini-haloes, therefore the following experiment can only be used to assess trends. However, since the model we consider in this work has stronger non-Gaussianity on smaller scales (and thus on less massive haloes), we can expect that the impact of non-Gaussianities on mini-haloes can be even larger than what we find (in the following paragraphs) for more massive haloes.

According to the Pop III star scenario, only metal-free haloes can host the first generation of stars. We therefore identify all the star-forming and metal-free haloes in the two simulations using the same approach described in Section 3.1. The probability of a halo being star forming is again $P_{SF} = 0.1$, identical for all redshifts, meaning that only 10 per cent of the haloes are selected in the first place as potential hosts of a Pop III remnant BH seed. Additionally,
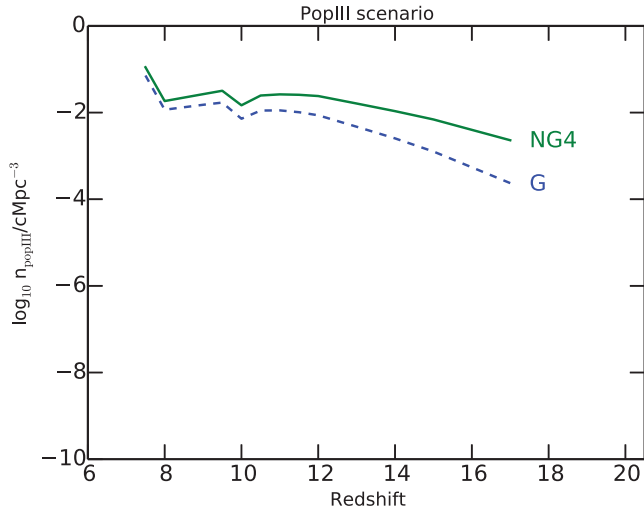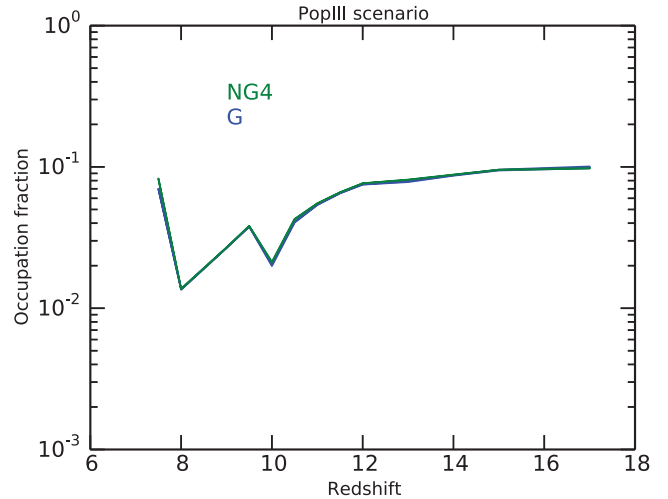
Figure 7. Number density of Pop III star remnant BHs formed at a given redshift for the Gaussian (dashed blue line) and the non-Gaussian (solid green line) simulations. Error bars represent the uncertainty of the mean value of the number density, the uncertainty is here too small to be seen.

Figure 8. Newly formed BH-halo occupation fraction for the Gaussian (blue line) and the non-Gaussian (green line) simulations, as a function of redshift, for the remnants of the first generation of stars scenario. As in Fig. 5, this is not a cumulative probability. Error bars represent the uncertainty of the mean value of the occupation fraction, the uncertainty is here too small to be seen.

we ensure that these haloes are not metal polluted from the past history of the halo (heritage pollution), nor from galactic winds coming from neighbouring haloes at a co-eval redshift.

Regarding the second aspect, we account for the probability of having a star-forming neighbour $P_{SF} = 0.1$ on a distance scale r_{bubble} defined in equation (11), this distance is redshift and halo mass dependent. We also consider the probability for the neighbouring haloes (on the same distance scale) to have spread metals in their past history, which could also have introduced metals in the considered halo, making it ineligible to form Pop III star in a metal-free environment. We perform 40 realizations of the model.

Fig. 7 represents the mean number density of potential BHs formed via the Pop III star remnant scenario for the two simulations (Gaussian in blue, non-Gaussian in green). The trends of the two curves are similar, but NG4 hosts more BHs. The enhancement in the number density of BHs increases with redshift, while at $z = 7.5$ the two curves are almost overlapping. However, the cumulative number density of BHs for NG4 is again almost twice as large (G: 0.17 cMpc^{-3}, NG4: 0.34 cMpc^{-3}). The cumulative number density in the two cases differs by more than $1 - \sigma$. The occupation fraction of haloes where BHs form via this scenario is shown in Fig. 8. The blue line indicates the occupation fraction for G, and the green line NG4. We note that the occupation fraction is almost identical for the two simulations: it is $\sim 10^{-1}$ at $z = 17$ and drops to $\sim 10^{-2}$ at $z = 8$ before increasing again (we account for forming BHs only, not the cumulative occupation fraction). The Gaussian case is slightly above the non-Gaussian one. This can be explained with the same arguments as those discussed for the DC case, and, moreover, haloes in NG4 have also a number of neighbours slightly higher than haloes in G, increasing the probability of being polluted by galactic winds. As noted above, our simulations do not resolve mini-haloes, but since our model for f_{NL} enhances the number of low-mass haloes at a given redshift, there will be more mini-haloes in the non-Gaussian case, favouring the formation of Pop III stars at even higher redshifts than those considered here. Therefore, also at higher redshift, the number of BHs formed throughout the Pop III remnant scenario would be higher in the non-Gaussian case until metal pollution starts dominating the environment. Our results can

therefore be considered a lower limit to the enhancement in the BH population.

5 BHS IN THE MOST MASSIVE HALOES AT $z = 6.5$

We now turn to exploring the possibility that the different growth histories of haloes in Gaussian and non-Gaussian models affect the assembly of BHs at the high-mass end. Using merger trees made with TREEMAKER, we derive the history of the most massive haloes in all simulation boxes at redshift $z = 6.5$. From the mass evolution of these haloes, we derive the evolution that a hypothetical BH in these haloes could have.

To probe the *cumulative* effect that a different early evolution has on the BH population, we evolve the BH masses in the merger trees. Rather than assigning a BH mass simply based on the halo mass at a given time we seed the highest redshift progenitor haloes of the $z = 6.5$ haloes with BH 'seeds' and evolve their mass over cosmic time adopting simple prescriptions. Our goal is to explore how the dominant differences in halo growth histories caused by non-Gaussian initial conditions affect the assembly of the BHs. The main diagnostics will be the mean BH mass as a function of time and the number of BHs with mass above some minimum threshold. The latter diagnostic is important as we are currently able to detect only the most massive BHs ($\sim 10^9$ M$_\odot$). Even in the future, at such high redshift, we will always pick the most massive BHs, although the mass threshold will decrease. For instance, the future X-ray mission ATHENA[2] is expected to be able to detect BHs with masses above 10^6–10^7 M$_\odot$ up to $z \sim 8$–10 (Aird et al. 2013).

Specifically, first we analyse the merger trees of all haloes with mass $> 10^{11}$ M$_\odot$ at $z = 6.5$ to find the effects of non-Gaussianities. There are 125 such haloes in simulation G and 133 in NG4. The main differences we find in the halo growth are in the total number of progenitors, and in the number of mergers involving similarly sized haloes, i.e. with mass ratio >0.1 ('major mergers' hereafter).

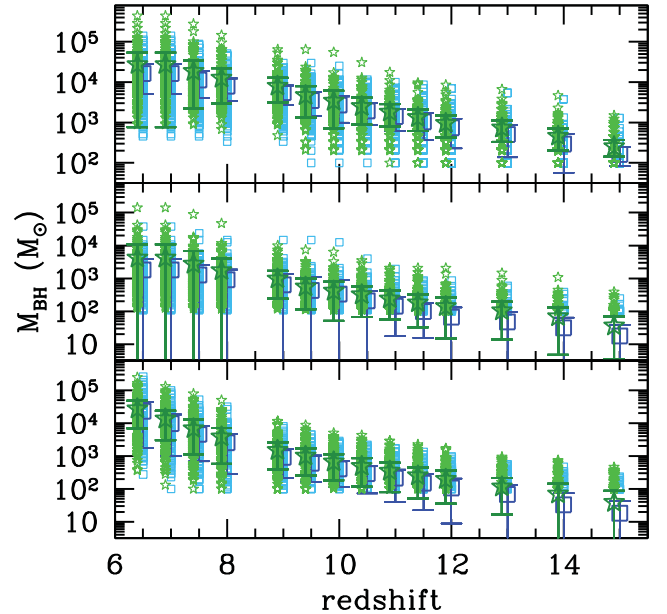[2] http://sci.esa.int/cosmic-vision/54517-athena/
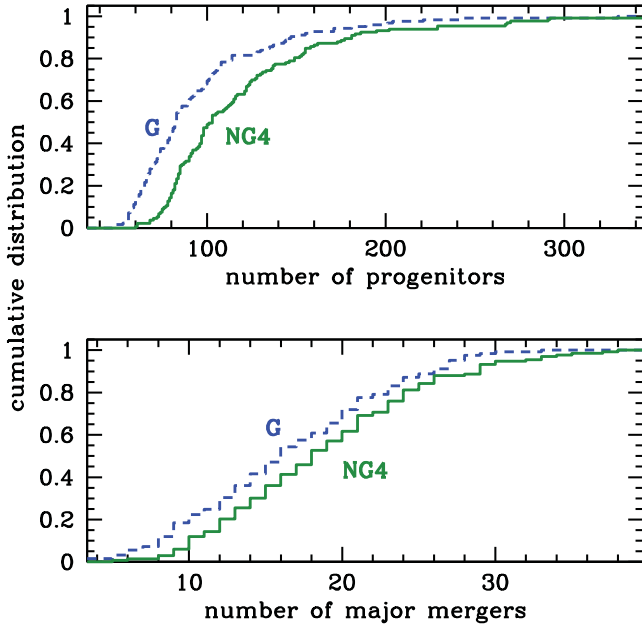
Figure 9. Cumulative distribution of the number of progenitors (top) and halo mergers with mass ratio >0.1 for all haloes with mass $> 10^{11}$ M$_\odot$ at $z = 6.5$ in the Gaussian (G, dotted blue histogram) and the non-Gaussian (NG4, green, solid histogram) simulations. The probability that the progenitor distributions come from the same parent distribution is less than 10^{-6}. The evidence for differences in the major merger distributions is weaker, 0.14.

Figure 10. Top: evolution of the BH mass for all haloes with mass $>10^{11}$ M$_\odot$ at $z = 6.5$, assuming that accretion is only merger driven. Middle: assuming the probability that a halo hosts a BH is 10 per cent, and accretion is only merger driven. Bottom: assuming that the probability that a halo hosts a BH is 10 per cent and BHs grow in mass through random accretion. Simulations: G (blue asterisks); NG4 (green stars). Each halo is represented by a point at each simulation output, and we calculate mean and variance at each output redshift (shown as a larger point with error bar).

We perform a Kolmogorov–Smirnov test (Fig. 9) and find that the probability that the progenitor number distributions come from the same parent distribution is less than 10^{-6}. The evidence for differences in the major merger distributions is weaker, with a probability of 0.14, because of the small-number statistics. The mean number of progenitors for the $> 10^{11}$ M$_\odot$ at $z = 6.5$ haloes is 95 for model G and 120 for NG4. The mean number of major mergers is 16 (G) and 20 (NG4).

We then model, in a simplified way, the evolution of hypothetical BHs over the cosmic history of these haloes. Two main factors linked to the different number of haloes and progenitors in G and NG4 would influence the BH distribution (masses and number) at $z = 6.5$: (i) how many haloes host BHs, and (ii) the number of major mergers for merger-driven BH growth. Regarding the first point, it is expected that BH formation is not ubiquitous in all haloes as specific conditions are required (see Sections 3 and 4 and Volonteri 2010, for a review). Therefore, if each halo has a given probability of hosting a BH, the larger the number of the progenitors of a halo, the higher the probability that a halo without a BH acquires a BH through a merger with a halo seeded by a BH (Menou, Haiman & Narayanan 2001). Regarding the second point, major galaxy mergers trigger torques that destabilize the gas in a galaxy, causing nuclear inflows that trigger BH accretion episodes (Kauffmann & Haehnelt 2000; Hopkins et al. 2006). If a BH is hosted in a galaxy that experiences a larger number of major mergers, its growth will be boosted.

To test how the different merger histories of Gaussian and non-Gaussian models affect the BH growth in this way, we perform a first experiment where we assume that each halo starts with a 10^2 M$_\odot$ BH, and, after each major merger, the BHs also accrete at the Eddington limit, assuming a radiative efficiency of 10 per cent, for one dynamical time (Tanaka 2014), while the masses of the BHs in the merging haloes are summed. The results are shown in Fig. 10, top panel. NG4 has a consistently higher mean BH mass

and a higher number of BHs with mass above a minimum threshold, e.g. 10^4 M$_\odot$ at $z = 6.5$. Simulation NG4 hosts 58 BHs with mass $>10^4$ M$_\odot$ at $z = 6.5$, while G hosts 57. The BHs with mass $>10^5$ M$_\odot$ are eight and three, respectively.

We perform a second experiment (Fig. 10, middle panel) where we assume that each halo has a 10 per cent probability of hosting a 10^2 M$_\odot$ BH when it enters the merger tree. We use here the occupation fraction of the Pop III star remnant case in order to have some statistics. We note that if we increased the seed mass by a given factor, the results shown below would scale by the same factor. Given the results of Sections 3 and 4, we adopt the same probability for both G and NG4. If the main halo already hosts a BH, the masses of the BHs in the main and merging halo are summed. BHs also accrete at the Eddington limit for one dynamical time after each major merger. Simulation NG4 has 12 BHs with mass $>10^4$ M$_\odot$ at $z = 6.5$, while G has 3. Above 10^5 M$_\odot$ are 1 and 0, respectively. By $z = 6.5$ 80 per cent of the haloes host a BH in G, while this fraction is 90 per cent for NG4, despite starting with the same occupation fraction of 10 per cent in each case (see Menou et al. 2001).

The final experiment is to forego major-merger-driven accretion and assign to each BH an accretion rate based on a distribution probability calculated in a large scale cosmological simulation, Horizon-AGN (Dubois et al. 2014). In Fig. 10, bottom panel, we show a model where we assume that each halo has a 10 per cent probability of hosting a 10^2 M$_\odot$ BH when it enters the merger tree, and if the main halo already hosts a BH, their masses are summed. The BHs also accrete over a timestep with an accretion rate randomly drawn from the distribution of Eddington rate, λ, calculated from all the BHs at $6 < z < 8$ in the Horizon-AGN simulation: $\mathrm{d}N/\mathrm{d}\log\lambda = 10^{(\log\lambda+2)}/10^2$. In this case, simulation NG4 hosts 67 BHs with mass $>10^4$ M$_\odot$ at $z = 6.5$ while G hosts 51. The BHs

with mass $>10^5\,\mathrm{M}_\odot$ are 10 and 9, respectively. Again, at $z = 6.5$ 80 per cent of the haloes host a BH in G, while this fraction is 90 per cent for NG4.

The main conclusion is that in NG4 the number of the most massive BHs is larger, and the mean BH mass at $z = 6.5$ increases by 0.08, 0.22, and 0.36 dex for the third, first, and second experiment, respectively. In the Eddington rate formalism, a mass difference of a factor of 2 corresponds to a change in the growth time of 70 per cent, because of the exponential dependence. While in all the experiments the statistical significance of the difference between G and NG4 is low (they are compatible within $1 - \sigma$) the trends are always consistent: if all conditions for BH growth are equal, i.e. BH physics is the same, a population of BHs in NG4 would grow faster and have more massive BHs. In the example shown here, however, the small high-redshift seeds do not grow much more than to a few $\times 10^5\,\mathrm{M}_\odot$ at $z = 6.5$. We have tested the difference with a case where the initial seed mass is $10^5\,\mathrm{M}_\odot$ (keeping all other assumptions equal), and we find that, in that case, BHs can grow up to several $10^8\,\mathrm{M}_\odot$, less than the masses of $z > 6$ quasars. This is not surprising, given the absence, in our simulation box, of the sufficiently massive DM haloes, $\sim 10^{13}\,\mathrm{M}_\odot$ expected to be hosting these extremely massive BHs. To explain the observed quasars, with mass $>10^9\,\mathrm{M}_\odot$, large seeds or additional growth channels (e.g. super-Eddington accretion), and sustained accretion at the Eddington level (Di Matteo et al. 2012; Dubois et al. 2012) would be needed.

6 DISCUSSION AND CONCLUSIONS

In this paper, we have addressed the formation and the growth of supermassive BHs in the presence of scale-dependent non-Gaussianities. We use two identical simulations except for their initial conditions, with either Gaussian or scale-dependent non-Gaussian primordial perturbations ($f_{\mathrm{NL}}(k) = f_{\mathrm{NL,0}}\,(k/k_0)^\alpha$, with $\alpha = 4/3$ and $f_{\mathrm{NL,0}} = 10^4$). The introduction of these non-Gaussianities on galactic scales, consistent at larger scales with the Planck results, produces an enhancement in the low-mass end of the halo and galaxy mass functions, increasing with redshift. As a consequence, changes in the BH population arise as well. We explore the impact of scale-dependent non-Gaussian primordial perturbations on two models of BH formation, and on the growth of the putative BHs. Sherkatghanad & Brandenberger (2015) also investigate local-type non-Gaussianities, i.e. with both skewness (f_{NL}) and kurtosis (described by the parameter g_{NL}), in the context of BH formation. They do not include scale-dependent non-Gaussianities, and conclude that non-Gaussianities do not strongly affect the number density of DM haloes at high redshifts (and of BHs as a consequence). This is in agreement with our previous work (Habouzit et al. 2014) where we showed that non-Gaussian models closest to a non-scale dependent f_{NL} do not show significant differences in halo and stellar mass functions compared to the Gaussian model. On a related note, Hirano et al. (2015a) find that varying the slope of the primordial power spectrum impacts the formation of structures as well: an enhanced power spectrum at small length-scales (or blue-tilted power spectrum) pushes to the formation of the first stars at much higher redshifts, and the higher CMB temperature leads to more massive stars, which can be precursor of massive BHs.

The formation of DC BHs is predicted to happen in metal-poor regions illuminated by a UV radiation intensity higher than a critical value (here we use $J_{\mathrm{21,LW,crit}} = 100$). We have implemented a model to identify these regions, inspired by D14, to compute the radiation

intensity emitted from galaxies forming in DM haloes. The increase in the galaxy mass function, particularly at the low-mass end, in the non-Gaussian simulation leads to a larger number density of potential DC regions. This is due to the increase of the number of galaxies for two reasons, there are statistically more regions that can collapse forming a BH, but also because more galaxies can act as radiation sources to illuminate dense regions where the collapse may happen. Conversely, the presence of more galaxies can also lead to a stronger metal enrichment, making a halo unavailable for the DC process. This last aspect has been difficult to study: we have implemented a model for the metal pollution coming from close star-forming regions, in the current time and the past history of the regions. Taking into account the pollution coming from galactic winds reveals a metal pollution of all the previously identified DC regions, making any comparison between the Gaussian and non-Gaussian simulations impossible. A larger simulation box would be needed to test in further detail the impact of the enhancement in the low-mass end of the galaxy mass function on the metal enrichment of potential DC regions by galactic winds.

However, as the critical value for the radiation intensity is still highly debated, and may be as high as $J_{\mathrm{21,LW,crit}} = 10^3$, only haloes as massive as $10^{11}\,\mathrm{M}_\odot$ or larger could provide sufficiently high radiation to suppress molecular hydrogen in their neighbourhood. The number of neighbours in the vicinity of the two haloes more massive than $10^{11}\,\mathrm{M}_\odot$ in the non-Gaussian simulation is larger, up to a factor 4, for haloes seeing a radiation intensity $>J_{\mathrm{21,LW}} = 500$ in the example shown in Fig. 6. This illustrates the effect of primordial non-Gaussianities in increasing the number density of DC regions. Metal pollution remains, however, a concern. Two factors may alleviate the importance of metal pollution: in the first place, SN bubbles may not be spherical, as assumed in D14 and our calculation, once a realistic gas and DM distribution is taken into account. Additionally, we and D14 have assumed, following Madau, Ferrara & Rees (2001) a simplified evolution of the bubble radius (see also section 5 in D14). A third approximation we and D14 have made is that the probability of a halo being star forming is constant with redshift and halo mass. These issues will be studied in a companion paper.

A second path for BH formation we have explored hinges on the remnants of the first generation of stars, in metal-free mini-haloes. In order to test the impact of primordial density perturbations on this scenario, we have modified the scheme we have adopted for the DC scenario (same probability for a halo to be star forming, and the same contributions for the metal pollution, namely pollution from heritage of the considered halo itself, and from galactic winds coming from neighbouring star-forming haloes). Only star-forming and metal-free haloes are considered as eligible site to form BHs. While our simulations have a much lower resolution than needed to resolve mini-haloes, we can at least identify some trends. We find that non-Gaussianities do not have a strong effect on the newly formed BH–halo occupation fraction, in both cases the occupation fraction drops from 10^{-1} at $z = 20$ to 10^{-2} at $z = 8$. Conversely, the number density of BHs is increased at the highest redshifts in the presence of non-Gaussianities, up to one order of magnitude. The larger number of progenitors and neighbours in the non-Gaussian simulation imply a larger probability for a halo to be/become polluted by metals.

The growth of supermassive BHs is also altered when considering non-Gaussianities. After deriving the merger history of the most massive haloes at $z = 6.5$ in both the Gaussian and non-Gaussian simulations, we study the evolution of BHs in massive haloes down to $z = 6.5$. To investigate the cumulative effect over cosmic times on the BHs assembly, we model the growth of BHs in three different

ways. Different probabilities for a halo of hosting a seed BH, and different accretion models (either each BH accretes at the Eddington limit for a dynamical time after a major merger or using an accretion rate based on a distribution probability derived from a large-scale hydrodynamical simulation) are adopted. We have not included in our models the effects of 'kicks' caused by asymmetric emission of gravitational waves, which have been proposed to be possibly responsible for ejecting BHs from haloes with shallow potential wells, thus halting or reducing the growth of high-redshift BHs hosted in small haloes (e.g. Yoo & Miralda-Escudé 2004; Volonteri & Rees 2006; Tanaka & Haiman 2009). This effect, however, seems to affect less than 10 per cent of binaries and it becomes negligible for BH mergers at $z < 10$ (Volonteri & Rees 2006). We find that non-Gaussianities imply a larger number of massive BHs and also an increase in the mean BH mass (up to 0.36 in the most favourable experiment). A population of supermassive BHs will then grow faster and to higher masses in a universe with scale-dependent non-Gaussian primordial density fluctuations. If the seed masses are similar to those of Pop III star remnants, BHs will not be able to grow above few $\times\ 10^5\ M_\odot$ by $z = 6$. However, our simulations do not resolve mini-haloes, and we may underestimate the growth of seeds at earlier times. We argue that, in a simulation resolving mini-haloes, BHs would have formed earlier through the Pop III remnant scenario, leading to a longer time for them to grow in mass. If we assumed that Pop III remnant seeds with mass $100\ M_\odot$ form at $z \sim 30$ in haloes unresolved in our simulations, they would have grown, assuming, optimistically, constant growth at the Eddington rate (but see Johnson & Bromm 2007; Alvarez, Wise & Abel 2009; Milosavljević, Couch & Bromm 2009; Park & Ricotti 2011) to $\sim 10^3\ M_\odot$ by $z = 18$, where we start our analysis. The final BH mass at $z = 6$ would then be $\sim$ one order of magnitude larger, a few $\times\ 10^6\ M_\odot$, still short of the $\sim 10^9\ M_\odot$ required. The very limited growth obtained for the Pop III remnant case suggests that large seeds or super-Eddington accretion (see Volonteri, Silk & Dubus 2015, and references therein) may be necessary for successful BH growth. We have done the same experiments on BH growth starting with initial $10^5\ M_\odot$ BH masses (not shown in the paper, but see Section 4). In this case we found that it is much easier for BHs to grow to higher BH masses, but still only to several $10^8\ M_\odot$. This is not unexpected, because our simulation box does not contain the very rare and biased DM haloes with masses $\sim 10^{13}\ M_\odot$ believed to be hosting these extreme BHs.

ACKNOWLEDGEMENTS

REFERENCES

Acquaviva V., Bartolo N., Matarrese S., Riotto A., 2003, Nucl. Phys. B, 667, 119
Agarwal B., Khochfar S., Johnson J. L., Neistein E., Dalla Vecchia C., Livio M., 2012, MNRAS, 425, 2854
Agarwal B., Vecchia C. D., Johnson J. L., Khochfar S., Paardekooper J.-P., 2014, MNRAS, 443, 648
Ahn K., Shapiro P. R., Iliev I. T., Mellema G., Pen U.-L., 2008, AIP Conf. Proc. Vol. 990, First Stars III. Am. Inst. Phys., New York, p. 374
Alishahiha M., Silverstein E., Tong D., 2004, Phys. Rev. D, 70, 123505
Aird J. et al., 2013, preprint (arXiv:1306.2325)
Alvarez M. A., Wise J. H., Abel T., 2009, ApJ, 701, L133
Aubert D., Pichon C., Colombi S., 2004, MNRAS, 352, 376
Ball W. H., Tout C. A., Żytkow A. N., Eldridge J. J., 2011, MNRAS, 414, 2751
Becker A., Huterer D., Kadota K., 2011, J. Cosmol. Astropart. Phys., 1, 6
Begelman M. C., 2010, MNRAS, 402, 673
Begelman M. C., Volonteri M., Rees M. J., 2006, MNRAS, 370, 289
Begelman M. C., Rossi E. M., Armitage P. J., 2008, MNRAS, 387, 1649
Behroozi P. S., Wechsler R. H., Conroy C., 2013, ApJ, 770, 57
Bromm V., Loeb A., 2003, ApJ, 596, 34
Bromm V., Yoshida N., 2011, ARA&A, 49, 373
Bruzual G., Charlot S., 2003, MNRAS, 344, 1000
Chen X., 2005, Phys. Rev. D, 72, 123518
Chevallard J., Silk J., Nishimichi T., Habouzit M., Mamon G. A., Peirani S., 2015, MNRAS, 446, 3235
Crocce M., Pueblas S., Scoccimarro R., 2006, MNRAS, 373, 369
Davies M. B., Miller M. C., Bellovary J. M., 2011, ApJ, 740, L42
Devecchi B., Volonteri M., 2009, ApJ, 694, 302
Di Matteo T., Khandai N., DeGraf C., Feng Y., Croft R. A. C., Lopez J., Springel V., 2012, ApJ, 745, L29
Dijkstra M., Haiman Z., Mesinger A., Wyithe S., 2008, MNRAS, 391, 1961
Dijkstra M., Ferrara A., Mesinger A., 2014, MNRAS, 442, 2036 (D14)
Dubois Y., Pichon C., Haehnelt M., Kimm T., Slyz A., Devriendt J., Pogosyan D., 2012, MNRAS, 423, 3616
Dubois Y. et al., 2014, MNRAS, 444, 1453
Fan X. et al., 2006, AJ, 132, 117
Fryer C. L., Woosley S. E., Heger A., 2001, ApJ, 550, 372
Gangui A., Lucchin F., Matarrese S., Mollerach S., 1994, ApJ, 430, 447
Habouzit M., Nishimichi T., Peirani S., Mamon G. A., Silk J., Chevallard J., 2014, MNRAS, 445, 129
Hirano S., Zhu N., Yoshida N., Spergel D., Yorke H. W., 2015a, ApJ, 814, 18
Hirano S., Hosokawa T., Yoshida N., Omukai K., Yorke H. W., 2015b, MNRAS, 448, 568
Hopkins P. F., Hernquist L., Cox T. J., Di Matteo T., Robertson B., Springel V., 2006, ApJS, 163, 1
Inayoshi K., Tanaka T. L., 2015, MNRAS, 450, 4350
Jiang L. et al., 2009, AJ, 138, 305
Johnson J. L., Bromm V., 2007, MNRAS, 374, 1557
Kauffmann G., Haehnelt M., 2000, MNRAS, 311, 576
Komatsu E., Spergel D. N., 2001, Phys. Rev. D, 63, 063002
Koushiappas S. M., Bullock J., Dekel A., 2004, MNRAS, 354, 292
Latif M. A., Volonteri M., 2015, MNRAS, 452, 1026
Latif M. A., Schleicher D. R. G., Schmidt W., Niemeyer J., 2013, MNRAS, 433, 1607
Latif M. A., Bovino S., Grassi T., Schleicher D. R. G., Spaans M., 2015, MNRAS, 446, 3163
Lewis A., Challinor A., Lasenby A., 2000, ApJ, 538, 473
Lodato G., Natarajan P., 2006, MNRAS, 371, 1813
Loeb A., Rasio F. A., 1994, ApJ, 432, 52
Madau P., Rees M. J., 2001, ApJ, 551, L27
Madau P., Ferrara A., Rees M. J., 2001, ApJ, 555, 92
Maldacena J., 2003, J. High Energy Phys., 5, 13
Menou K., Haiman Z., Narayanan V. K., 2001, ApJ, 558, 535
Milosavljević M., Couch S. M., Bromm V., 2009, ApJ, 696, L146
Mortlock D. J. et al., 2011, Nature, 474, 616
Mutch S. J., Croton D. J., Poole G. B., 2013, MNRAS, 435, 2445
Nishimichi T., 2012, J. Cosmol. Astropart. Phys., 8, 37
Nishimichi T. et al., 2009, PASJ, 61, 321
Park K., Ricotti M., 2011, ApJ, 739, 2
Planck Collaboration XVI, 2014a, A&A, 571, A16
Planck Collaboration XXIV, 2014b, A&A, 571, A24
Redmount I. H., Rees M. J., 1989, Comments Astrophys., 14, 165
Regan J. A., Johansson P. H., Wise J. H., 2014, ApJ, 795, 137

Schnittman J. D., 2007, ApJ, 667, L133

Scoccimarro R., 1998, MNRAS, 299, 1097

Shakura N. I., Sunyaev R. A., 1973, A&A, 24, 337

Shang C., Bryan G. L., Haiman Z., 2010, MNRAS, 402, 1249

Sherkatghanad Z., Brandenberger R. H., 2015, preprint (arXiv:1508.00968)

Silverstein E., Tong D., 2004, Phys. Rev. D, 70, 103505

Spaans M., Silk J., 2006, ApJ, 652, 902

Springel V., 2005, MNRAS, 364, 1105

Sugimura K., Omukai K., Inoue A. K., 2014, MNRAS, 445, 544

Tanaka T. L., 2014, Class. Quantum Gravity, 31, 244005

Tanaka T., Haiman Z., 2009, ApJ, 696, 1798

Tweed D., Devriendt J., Blaizot J., Colombi S., Slyz A., 2009, A&A, 506, 647

Valageas P., Nishimichi T., 2011, A&A, 527, A87

Volonteri M., 2010, A&AR, 18, 279

Volonteri M., Rees M. J., 2006, ApJ, 650, 669

Volonteri M., Madau P., Haardt F., 2003, ApJ, 593, 661

Volonteri M., Silk J., Dubus G., 2015, ApJ, 804, 148

Wu X.-B. et al., 2015, Nature, 518, 512

Yoo J., Miralda-Escudé J., 2004, ApJ, 614, L25

This paper has been typeset from a TEX/LATEX file prepared by the author.